Eur. Phys. J. B **12**, 367–372 (1999)

THE EUROPEAN PHYSICAL JOURNAL B

EDP Sciences

Analysis of infrared reflectivity of conducting polymers: example of camphor-sulphonic-acid-doped polyaniline

N. Petit[1], F. Gervais[1,a], P. Buvat[2], P. Hourquebie[2], and P. Topart[2]

[1] Laboratoire d'Électrodynamique des Matériaux Avancés[b], Université François Rabelais, Parc de Grandmont, 37200 Tours, France
[2] CEA/Le Ripault, Département Matériaux, BP 16, 37260 Monts, France

Received 11 February 1999 and Received in final form 26 April 1999

Abstract. The reflectivity spectrum of a polyaniline CSA-doped in presence of m-cresol has been measured over the wide wavenumber range of 15–9 000 cm^{-1} (0.002–1.1 eV) at room temperature. Experimental data compare well with similar experiments performed by another group. The conductivity spectrum of this conducting polymer has been deduced from the reflectivity spectrum by means of two methods, Kramers-Kronig transformation and best fit of an "extended Drude" model to the reflectivity spectrum. Whereas the deviation from Drude behavior was interpreted in terms of Anderson localization or by inhomogeneous disorder by other groups, it is shown here that a different model developed for conducting oxides that also exhibit non-Drude behavior, applies very well to this example of conducting polymer.

PACS. 78.30.Jw Organic compounds, polymers – 72.80.Le Polymers; organic compounds (including organic semiconductors) – 71.38.+i Polarons and electron-phonon interactions

1 Introduction

Whereas conventional metallic materials show an infrared-visible-near UV conductivity spectrum that is generally well described by the Drude model, studies of conducting oxides performed during the ten last years have shown the general non-Drude behavior of non-metal conductors. This is true in particular for high-T_c cuprate superconductors [1–4], which have been the subject of extensive studies, but also more recently for manganite-type systems that display giant magneto-resistance (GMR) phenomena [5]. The conventional Drude model applies to coherent motions of "free electrons" in systems in which screening assumes vanishingly small interaction between charge carriers, expressed for example *via* the Thomas-Fermi vector. However, the screening is generally incomplete in conducting oxides and in conducting polymers as well [6], as probed by the signature of polar phonon in infrared reflectivity spectra. This is, at least partly, the consequence of lower carrier densities, compared to conventional metals. There are at least two important consequences of this incomplete screening: (i) the relevance of possible polaronic conductivity mechanism instead of free electron model for polar media in which the Coulombic field is no longer negligible, (ii) the incomplete Thomas-Fermi exponential decay consequences, such as possible interactions of charge carriers. This means that the electronic transport mechanism in conducting materials that deviate from conventional metals has to be considered specifically in the intermediate carrier density regime. This is particularly important in the conditions of incomplete screening because this general framework is applicable to many classes of materials of high interest such as conducting oxide ceramics, films, oxide superconductors, GMR materials, and conducting polymers. An example in the case of the latest type of materials is presented here. Conjugated polymers have attracted considerable interest in applied and fundamental research since the discovery of conductivity in doped polyacetylene in 1977 [7]. Since then, an enormous amount of efforts has gone toward the understanding of the electronic and transport properties in conjugated polymers. Within the class of conducting polymers, polyaniline (PANI) is unique in that the electronic structure and electrical properties can be reversibly controlled both by charge transfer doping and by protonation [8]. The wide range of associated electrical and optical properties coupled with excellent environmental and thermal stability, make polyaniline attractive as an electronic material for potential use in a variety of applications. Recently, progress in the synthesis and processing of the polyaniline protonated with camphor sulfonic acid (PANI-CSA) in meta-cresol has greatly improved the homogeneity of the material and significantly

[a] e-mail: gervais@delphi.phys.univ-tours.fr
[b] Laboratoire de Recherche Correspondant du CEA LRC M01

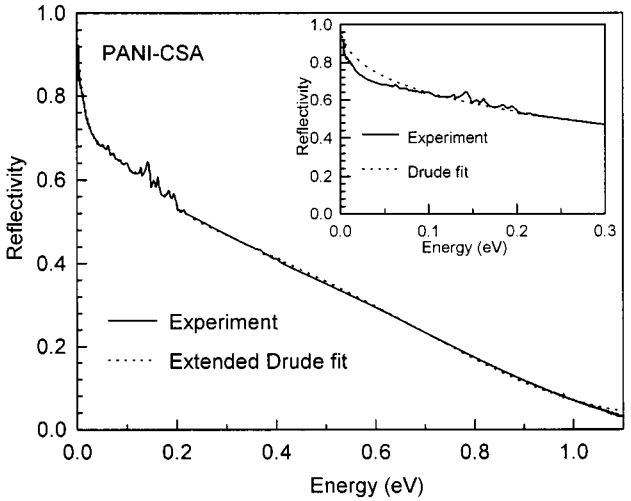

Fig. 1. Reflectivity spectrum of an 8 μm-thick PANI-CSA film at room temperature (solid curve). The dotted line represents the best fit obtained with the "extended-Drude model". The fit parameters used are given in Table 1. The inset shows a fit with a conventional Drude model without fitting the phonons: the agreement is good for the higher energies but is not satisfactory in the far-infrared region.

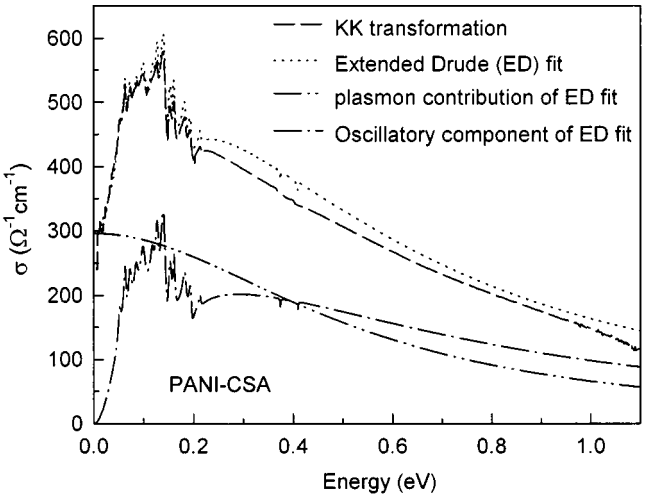

Fig. 2. Optical conductivity $\sigma(\omega)$ of PANI-CSA calculated from the KK transformation of the reflectivity data (dashed line) compared with that obtained from the ED fit (dotted line) as described in equation (2). The ED model allows the separation of the oscillatory component of the spectral conductivity from the plasmon contribution.

reduced the degree of structural disorder [9]. These structurally improved materials provide opportunities to study the Metal-Insulating transition and the intrinsic metallic state focusing on the role of disorder on localization phenomena [6,10–12].

2 Experiments

The emeraldine base form of the polyaniline was synthesized chemically according to reference [13] by the oxidative polymerization of aniline in an aqueous HCl solution. The mixture of aniline and ammonium persulfate was stirred for 72 hours at −40 °C. PANI-CSA doped polymer was then prepared by mixing two equivalents of emeraldine base and one equivalent of camphor sulfonic acid. The molar ratio of CSA to phenyl-nitrogen repeat unit was 0.5 for complete protonation of the polyaniline to the emeraldine salt form [14]. High quality films of PANI-CSA were then obtained by casting the material from solution in meta-cresol [14]. Films were then air dried for 48 h at 50 °C. The thickness of the film investigated here is 8 μm. It is sufficiently larger than the electromagnetic penetration depth to avoid the transmittance of the incident radiation as will be checked later on. The reflectivity spectrum of the polymer film was measured at room temperature with an IFS 113 Bruker infrared Fourier transform spectrometer in the wavenumber range 15–9 000 cm^{-1}.

3 Results and discussion

The reflectivity spectrum is shown in Figure 1. It is characteristic of a conducting material with a reflectivity which tends towards 100% in the lower energy region. The spectrum is similar to that reported in reference [6]. Our overall reflectivity is a few percent higher than that of the sample of reference [6]. DC conductivities are also similar, 200 $s\,cm^{-1}$ for our sample. The optical conductivity was first obtained by the Kramers-Kronig (KK) transformation as shown in Figure 2 (dashed lines). Note that the conductivity rate can vary significantly depending on the experimental data range used for the calculation. As a result, this type of calculation may introduce serious errors if there is some remaining dispersion outside the experimental data range. KK transformation is well adapted to insulating materials because one can select a data range with a flat reflectivity at both ends such that there is no remaining dispersion outside the experimental range. Conversely, in conducting media, the response remains nonzero down to zero frequency.

3.1 Fit model

In most conducting oxides, the usual Drude model is unable to fit the experimental reflectivity. The same was already reported in the conducting polymer studied in reference [6]. A "localization-modified Drude" (LMD) model was proposed to overcome this difficulty. Here, an alternative is tested, inherited from previous studies of conducting oxide materials. An "extended Drude" model, derived from the factorized form of the dielectric function, has been introduced to try to reconcile experiment and phenomenological Drude-type approach. This model is based upon the extension of the Lyddane-Sachs-Teller relationship

Table 1. Fitting parameters and oscillator strengths of transverse ($\Delta\varepsilon_j$) and longitudinal ($\Delta\eta_j$) modes calculated from the TO–LO splitting.

Oscillation Parameters					
Ω_{TO} (cm^{-1})	γ_{TO} (cm^{-1})	Ω_{LO} (cm^{-1})	γ_{LO} (cm^{-1})	$\Delta\varepsilon_j$	$\Delta\eta_j$ ($x10^{-4}$)
420	47	425	50	0.94	4.5
512	49	520	48	1.47	6.9
588	74	600	83	1.51	9.5
689	79	697	87	0.90	5.7
805	104	820	118	1.48	9.3
952	58	956	61	0.35	1.6
1035	46	1041	48	0.62	2.2
1151	81	1178	62	2.56	7.0
1237	72	1259	90	1.33	8.1
1297	43	1300	69	1.41	1.5
1483	70	1493	75	0.94	1.7
1572	43	1579	44	0.72	1.0
1720	36	1721	39	0.36	0.1
1800	6459	6038	6695	21.72	3639.9
3018	13	3017	12	$7.5\ 10^{-4}$	0.1
3300	23	3299	22	$2.5\ 10^{-3}$	0.4
Plasmon Parameters (cm^{-1})			ε_∞=2.52		
Ω_P	γ_0	γ_P			
5500	4300	4300			

in the form

$$\tilde{\varepsilon} = \varepsilon_\infty \prod_j \frac{\Omega_{j\mathrm{LO}}^2 - \omega^2 + \mathrm{i}\gamma_{j\mathrm{LO}}\omega}{\Omega_{j\mathrm{TO}} - \omega^2 + \mathrm{i}\gamma_{j\mathrm{TO}}\omega} \tag{1}$$

which expresses that longitudinal optical modes are the complex zeroes of the dielectric response, while the transverse modes are its complex poles. This is a straightforward application of one of the Maxwell relationships. In equation (1), Ω represent the frequencies and γ the damping of each oscillator j, respectively, and $\varepsilon_\infty = 1 + \chi_{\mathrm{electronic}}$ is the "high-frequency" dielectric constant from the viewpoint of the IR spectroscopist. The general formula, which permits to separate the contribution of charge carrier motion (*i.e.* without restoring force) and of the other excitations (such as phonons, trapped polarons), can be written as

$$\tilde{\varepsilon} = \varepsilon_\infty \left[\prod_j \frac{\Omega_{j\mathrm{LO}}^2 - \omega^2 + \mathrm{i}\gamma_{j\mathrm{LO}}\omega}{\Omega_{j\mathrm{TO}}^2 - \omega^2 + \mathrm{i}\gamma_{j\mathrm{TO}}\omega} - \frac{\Omega_\mathrm{P}^2 + \mathrm{i}(\gamma_\mathrm{P} - \gamma_0)\omega}{\omega(\omega - \mathrm{i}\gamma_0)} \right] \tag{2}$$

where Ω_P is the plasma frequency defined *via*

$$\Omega_\mathrm{P}^2 = \frac{ne^2}{m^*\varepsilon_\mathrm{v}\varepsilon_\infty} \tag{3}$$

γ_P represents the linewidth of the plasma response centered at $\omega = \Omega_\mathrm{P}$ and γ_0 is the linewidth of the absorption centered at $\omega = 0$. One recovers the usual Drude model on setting $\gamma_0 = \gamma_\mathrm{P}$. The reflectivity is then calculated from the dielectric function *via*

$$R = \left| \left(\sqrt{\tilde{\varepsilon}} - 1\right) \Big/ \left(\sqrt{\tilde{\varepsilon}} + 1\right) \right|^2 \tag{4}$$

and the spectral conductivity $\tilde{\sigma}$ *via*

$$\tilde{\varepsilon} = 1 - \frac{\mathrm{i}\tilde{\sigma}}{\varepsilon_\mathrm{v}\omega} \tag{5}$$

where ε_v is the dielectric constant of vacuum. This "extended-Drude" (ED) model has been shown to yield much better fit than usual Drude model for conducting oxide materials like reduced TiO_2 [15], NbO_2 [16,17], $SrTiO_3$ either reduced [1] or Nb-doped [18] lanthanum [19] and praseodymium [20] nickelates, $BaBiO_3$ [2] and various cuprates [3,4] and also manganites [5]. It was tempting to try to apply this model to a conducting polymer, the spectrum of which does not exhibit usual Drude-type profile. The best compromise with the usual Drude model is shown in the inset of Figure 1. A significant improvement is achieved by increasing γ_0 with respect to γ_P in equation (2). But, on this basis, one cannot reproduce the decrease of spectral conductivity below 0.12 eV (Fig. 2). To achieve a good fit with the ED model requires adding a broad oscillator near 0.22 eV. The behavior is, therefore, confirmed not to be typical of usual Drude because the fit requires an extra contribution in the form of an additional broad band the spectral weight of which is about one half of the total conductivity. In Figure 1, the agreement of the fit with the experimental spectrum is quite good over the whole range. The fitting parameters are given in Table 1. In Figure 2, the optical conductivity calculated from the parameters, which yield the best fit to the reflectivity data, is in good agreement with the KK data. The high-frequency reflectivity has not been fitted either, but evaluated from the calculation of the square of the refractive index in the visible region, namely $\varepsilon_\infty \approx 2.52$. The calculated reflectivity above 1.1 eV compares well the data of reference [6]. This type of data fit allows a parametrization that could make possible the comparison between different classes of materials, in particular oxides. From the best fit, we have deduced the real part of the optical conductivity of the sample as seen in Figure 2 (dotted line). The oscillatory component of the conductivity and the non-oscillatory plasmon contribution, whose characteristics fix the static value of the conductivity, are shown separately in Figure 2. The static value of the conductivity deduced from the fit $\sigma(\omega = 0) \approx 300\ \Omega^{-1}\mathrm{cm}^{-1}$ is consistent with the measured DC conductivity $\sigma(\omega = 0) \approx 200\ \Omega^{-1}\mathrm{cm}^{-1}$.

3.2 Phonons

Our procedure first allows a parametrization of phonon parameters. The phonon dampings are found rather large for organic materials. This may be an indication of the effect of structural disorder. Note that, to the best of our knowledge, this is the first attempt of fitting of the phonon spectrum in a conducting polymer. In reference [12], the authors fitted the broad reflectivity profile with a localisation-modified Drude model (LMD) [10], but did not fit the phonons. Figure 3, which displays a magnification in the phonon spectral range, shows that

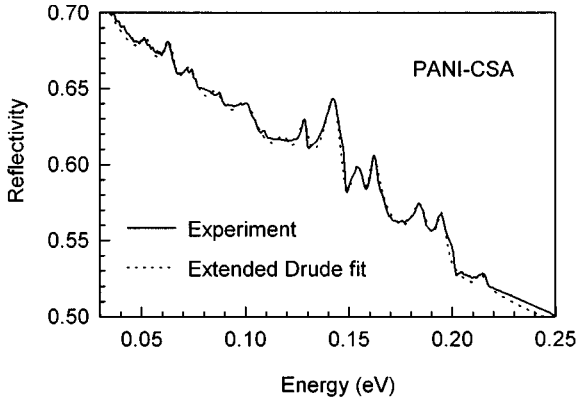

Fig. 3. Reflectivity spectrum of PANI-CSA at room temperature (experimental data and fit): zoom of the phonon region.

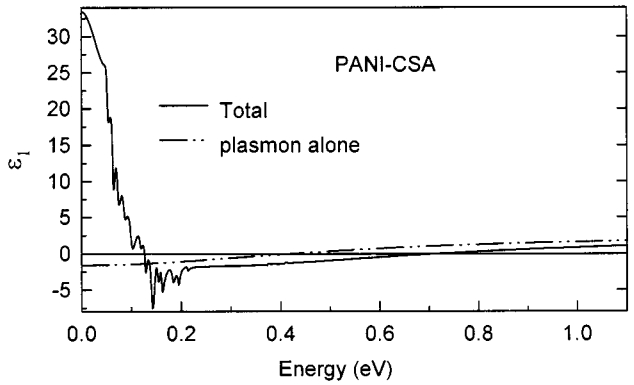

Fig. 4. The real part ε_1 of the dielectric function, $\varepsilon(\omega) = \varepsilon_1 - \mathrm{i}\varepsilon_2$, of PANI-CSA obtained from the ED fit of the reflectivity data. ε_1 is positive in the far-infrared region contrary to expectations of the conventional Drude model; it crosses zero twice, at ~ 0.13 eV and again at ~ 0.72 eV.

the agreement of the calculated curve with experiment is excellent. In Table 1, the oscillator strengths are not fitting parameters. The oscillator strengths of transverse ($\Delta\varepsilon_j$) and longitudinal ($\Delta\eta_j$) modes are calculated from the TO–LO splittings *via*

$$\Delta\varepsilon_j = \frac{\varepsilon_\infty}{\Omega^2_{j\mathrm{TO}}} \frac{\prod_k \left(\Omega^2_{k\mathrm{LO}} - \Omega^2_{j\mathrm{TO}}\right)}{\prod_{k\neq j} \left(\Omega^2_{k\mathrm{TO}} - \Omega^2_{j\mathrm{TO}}\right)}$$

$$\text{and } \Delta\eta_j = \frac{1}{\varepsilon_\infty \Omega^2_{j\mathrm{LO}}} \frac{\prod_k \left(\Omega^2_{k\mathrm{TO}} - \Omega^2_{j\mathrm{LO}}\right)}{\prod_{k\neq j} \left(\Omega^2_{k\mathrm{LO}} - \Omega^2_{j\mathrm{LO}}\right)} \quad (6)$$

3.3 Optical conductivity

The plasmon-like contribution is highly damped. It is not overdamped however. As a result, the sole plasmon contribution to the real part of the dielectric response, plotted separately in Figure 4, is negative below the plasma frequency parameter, as expected for a Drude contribution. The plasmon contribution shown separately in Figure 2 is maximum at zero frequency, as expected. The oscillatory part of the conductivity shows a broad bump near 0.28 eV. Such bumps in comparable energy ranges were observed in the conductivity spectra of certain conducting oxides. In the specific case of Pr_2NiO_4, they were shown to be compatible with the signature of polarons [20]. More specifically, one may consider small polaron bands, which may lie at high energies (lower than the energy gap), and trapped-large-polaron bands. By "trapped-large-polarons", we mean the charges that remain localized below the mobility edge by disorder [6,11,21–25] or any other physical reason. Even in the absence of localization by disorder, the band of large-trapped-polarons is observed for non-metallic conducting oxides in the mid-infrared [20]. Localization by disorder of course reinforces this possibility. In the case of conducting polymers, this mid-infrared band is expected, therefore, to be broad. This is just what is observed *via* our additional broad oscillator (TO mode at 0.22 eV, LO mode at 0.75 eV). The average frequency, 0.5 eV, is of the same order of magnitude of what is observed in conducting oxides [1,20]. Present results, therefore, confirm that the polaronic scenario should be considered to understand the high-frequency (infrared) conductivity mechanism of conducting polymers, as in the present example. The application of the relationship

$$\int_0^\omega \sigma(\omega')\mathrm{d}\omega' = \frac{\pi e^2}{2} \frac{N_{\mathrm{eff}}(\omega)}{m^*} \quad (7)$$

allows to estimate $N_{\mathrm{eff}} = 1.2 \times 10^{21}$ e/cm^3 upon integrating our optical conductivity up to $\omega = 9\,000$ cm^{-1} if one assumes that the electron effective mass m^* is the electron mass. Within the same integration range and with the same assumption for the effective mass, one finds $N_{\mathrm{eff}} = 0.85 \times 10^{21}$ e/cm^3 by using equation (3). It is consistently smaller than the result *via* (7) since only mobile charge carriers contribute to the second determination. We check, therefore, that the electronic density is significantly lower than that of normal metals ($> 10^{22}$ e/cm^3) but is comparable with that ($\sim 10^{21}$ e/cm^3) of high-T_c oxide superconductors. The imaginary part of the inverse dielectric function shown in Figure 5 shows a maximum near 0.9 eV. This is slightly higher than the plasma frequency (0.7 eV), due to coupling with LO oscillators (mainly the 0.75 eV bump) and the highly-damped character of the plasmon. The spectrum of the absorption coefficient of our sample is displayed in Figure 6. The inverse absorption coefficient K^{-1} is the penetration depth of the radiation. We check that the sample thickness, 8 μm, is larger than K^{-1} in the whole investigated spectral range.

There is however an alternative to the present approach which is, for instance, exemplified in several works [11,12]. A localization of carriers by disorder is assumed to decrease the Drude contribution towards low

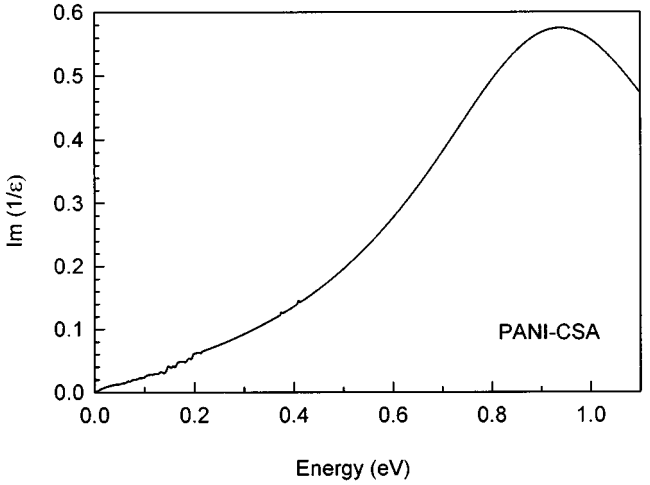

Fig. 5. Energy-loss function $\Im[1/\varepsilon(\omega)]$ of PANI-CSA calculated from the dielectric function deduced from the ED fit of the reflectivity spectrum.

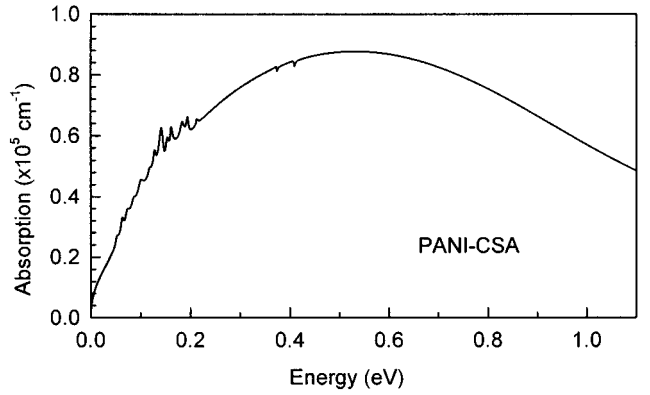

Fig. 6. The absorption coefficient spectrum K^{-1} of PANI-CSA deduced from the ED fit of the reflectivity spectrum. In the investigated spectral range, K^{-1} (the penetration depth) is larger than the thickness of the PANI-CSA-film studied (8 μm).

frequencies in the form

$$\sigma_{\mathrm{LMD}}(\omega) = \sigma_{\mathrm{D}}(\omega)\left\{1 - \left[1 - (3\tau\omega)^{1/2}\right] \Big/ (k_{\mathrm{F}}l)^2\right\} \quad (8)$$

where τ is the carrier relaxation time, k_{F} the Fermi vector and l the carrier mean free path. There are at least two ways to discriminate between models, extended-Drude and LMD. One is to check whether or not the charge carriers screen the phonons correctly. The result is satisfactory with our extended-Drude model. Conversely, it has not been checked with the LMD model to our knowledge. A more complete way to discriminate them would be to compare the fit quality (with phonon fitting) by varying the doping upon a wide range. This is planned in a near future.

4 Conclusion

The reflectivity of a film of CSA-doped polyaniline has been investigated in terms of spectral conductivity, both by Kramers-Kronig transformation and fitting procedure. Both approaches compare well. At low energy, the experimental reflectivity tends towards 100% as expected for a conventional metal. However, the analysis of the spectral conductivity shows significant deviation from the Drude behavior because the response contains two main contributions: (i) a highly-damped plasmon-like contribution and (ii) a broad additional oscillator centered at 0.5 eV which amounts to one half of the total spectral weight. Comparison with similar observations of a mid-infrared band in conducting oxides suggests a polaronic origin for this additional contribution. A general theory of conductivity in media at intermediate charge carrier density, valid for conducting polymers or oxides or other non-metal conducting media appears highly desirable. Within this perspective, the parametrization of the conductivity performed here will be useful for comparison with different classes of materials. Our model introduces a perspective, which is complementary of other models published. The previous views of Anderson localization [10] proposed to account for the deviation from the Drude prediction of both reflectivity and conductivity at low energies, has been criticised by more recent studies [25] which rather suggest an inhomogeneous disorder. Our approach is compatible with this view. It has the merit in addition to suggest a method to discriminate between trapped and mobile charge carriers. Further planned studies *versus* temperature and doping will allow us to complement this original approach and possibly to discriminate with the LMD model.

References

1. F. Gervais, P. Echegut, J.M. Bassat, P. Odier, Phys. Rev. B **37**, 9364 (1988).
2. R.P.S.M. Lobo, F. Gervais, Phys. Rev. B **52**, 13294 (1995).
3. R.P.S.M. Lobo, F. Gervais, C. Champeaux, P. Marchet, A. Catherinot, Mat. Sci. Eng. B **34**, 74 (1995).
4. R.P.S.M. Lobo, F.J. Gotor, P. Odier, F. Gervais, Phys. Rev. B **53**, 410 (1997).
5. F. Gervais, C. Daulan, A. Maignan, R. Lobo, Int. J. Mod. Phys. B **12**, 3393 (1998).
6. K. Lee, A.J. Heeger, Y. Cao, Phys. Rev. B **48**, 14 884 (1993).
7. C.K. Chiang, C.R. Fincher Jr., Y.W. Park, A.J. Heeger, H. Shirakawa, E.J. Louis, S.C. Gau, A.G. MacDiarmid, Phys. Rev. Lett. **39**, 1098 (1977).
8. W.R. Salaneck, I. Lundstrom, W.S. Huang, A.G. MacDiarmid, Synth. Met. **13**, 291 (1986).
9. A.G. MacDiarmid, A.J. Epstein, Synth. Met. **65**, 103 (1994).
10. P.W. Anderson, Phys. Rev. **109**, 1492 (1958).

11. A.J. Epstein, J. Joo, R.S. Kohlman, G. Du, E.J. Oh, Y. Min, J. Tsukamoto, H. Haneko, J.P. Pouget, Synth. Met. **65**, 149 (1994); R.S. Kohlman, T. Ishiguro, H. Haneko, A.J. Epstein, Synth. Met. **69**, 325 (1995); Y. Xia, J. Joo, A.G. MacDiarmid, A.J. Epstein, Macromolecules **27**, 7212 (1994); K. Lee, M. Reghu, C.O. Yoon, A.J. Heeger, Phys. Rev. B **52**, 4779 (1993); P. Buvat, Thèse, Université Villetanneuse 1997; L. Olmedo, P. Buvat, P. Hourquebie, F. Lubrano (to be presented to Antech'99); P. Topart, P. Hourquebie (to be submitted to Thin Solid Films).
12. K. Lee, E.K. Miller, A.N. Aleshin, R. Menon, A.J. Heeger, J.H. Kim, C. O. Yoon, H. Lee, Adv. Mater. **10**, 456 (1998).
13. Y. Cao, A.J. Heeger *et al.*, Polymer **30**, 2305 (1989); P. Hourquebie, B. Blondel, S. Dhume, Synt. Met. **85**, 1437 (1997).
14. Y. Cao, G.M. Treacy, P. Smith, A.J. Heeger, Phys. Rev. B **48**, 17685 (1993).
15. J.F. Baumard, F. Gervais, Phys. Rev. B **15**, 2316 (1977).
16. F. Gervais, Phys. Rev. B **23**, 6580 (1981).
17. F. Gervais, in *Infrared and Millimeter Waves*, edited by K.J. Button (Academic Press, New York, 1983), Vol. 8, pp. 279–339.
18. F. Gervais, J.L. Servoin, A. Baratoff, J.G. Bednorz, G. Binnig, Phys. Rev. B **47**, 8187 (1993).
19. J.M. Bassat, P. Odier, F. Gervais, Phys. Rev. B **35**, 7126 (1987).
20. D. Eagles, R.P.S.M. Lobo, F. Gervais, Phys. Rev. B **52**, 6440 (1995).
21. N.F. Mott, M. Kaveh, Adv. Phys. **34**, 329 (1985).
22. M. Reghu, Y. Cao, D. Moses, A.J. Heeger, Phys. Rev. B **47**, 1758 (1993).
23. J. Joo, V.N. Prigodin, Y.G. Min, A.G. MacDiarmid, A.J. Epstein, Phys. Rev. B **50**, 12226 (1994).
24. A.J. Epstein, J. Joo, R.S. Kohlman, G. Du, E.J. Oh, Y. Min, J. Tsukamoto, H. Haneko, J.P. Pouget, Synth. Met. **65**, 149 (1994).
25. R.S. Kohlman, J. Joo, Y.G. Min, A.G. MacDiarmid, A.J. Epstein, Phys. Rev. Lett. **77**, 2766 (1996).